New Insight into Cellulose Structure by Atomic Force Microscopy Shows the I_α Crystal Phase at Near-Atomic Resolution

A. A. Baker,* W. Helbert,† J. Sugiyama,‡ and M. J. Miles*

*H. H. Wills Physics Laboratory, University of Bristol, Bristol BS8 1TL, United Kingdom; †Centre de Recherches sur les Macromolécules Végétales, Centre National de la Recherche Scientifique, 38041 Grenoble Cedex 9, France; and ‡Wood Research Institute, Kyoto University, Uji, Kyoto 611-0011, Japan

ABSTRACT The organization of the surface of cellulose is important in cell structure, as well as in industrial processing and modification. Using atomic force microscopy, we show that the I_α phase of native cellulose first proposed in 1984 and subsequently characterized by a triclinic unit cell exists over large areas of the surface of microcrystals from *Valonia*, one of the most highly crystalline celluloses. There is startling agreement between the observed structure and crystal models, and it is possible to identify the specific crystal face being imaged. The near-atomic resolution images also offer an insight into structural reconstructions at the surface compared to the interior. We are able to assign features in the images to particular side groups attached to the glucose ring and find indications of subtle modifications of the position of surface hydroxyls due to changes in hydrogen bonding.

INTRODUCTION

Understanding the details of cellulose structure is increasingly important as the drive to use renewable resources in technological applications increases. Techniques that have probed cellulose structure have so far been of limited applicability in describing the cellulose surface, which is vitally important in many natural and industrial processes, such as enzymic hydrolysis. Scanning probe microscopy techniques, particularly atomic force microscopy (AFM), are unique in their ability to obtain high-resolution images of the surface of biological specimens under liquids. In this paper, we use AFM to compare the surface of cellulose with its crystalline interior and to demonstrate the similarities and differences that exist between them.

Native crystalline cellulose comprises chains arranged in parallel with a twofold screw symmetry along the chains due to the β-[1,4] linkage of the D-glucose subunits. It is now widely accepted that two phases coexist within native cellulose I, known as I_α and I_β, first discovered by the analysis of spectral line splitting in solid-state ^{13}C cross-polarization/magic angle spinning NMR spectroscopy (Atalla and VanderHart, 1984; VanderHart and Atalla, 1984). Crystallographic studies have indexed these phases with one-chain triclinic and two-chain monoclinic unit cells, respectively (Sugiyama et al., 1990). The triclinic unit cell of Sugiyama et al. (1991), first suggested by Sarko and Muggli as a two-chain cell (Sarko and Muggli, 1974), has a single-chain P1 structure, with adjacent molecules shifted monotonically by one-quarter of the unit cell size in the *c* direction. In the two-chain monoclinic unit cell, the corner chain is shifted *c*/4 relative to the center chain, such that the overall configuration displays staggering of adjacent chains. It is not clear why there are two different crystalline allomorphs, previously shown to coexist within single microfibrils (Sugiyama et al., 1991), although stresses present during biosynthesis have been implicated (Sugiyama et al., 1990, 1991; Horii et al., 1997). The I_α phase, dominant in algal and bacterial cellulose, is metastable and may be transformed into I_β via a hydrothermal annealing treatment (Yamamoto et al., 1989). Cellulose from the green alga *Valonia ventricosa* that was used in this study is estimated to be approximately two-thirds I_α phase in the bulk (VanderHart and Atalla, 1984). Previous studies have shown that the I_α phase exists in small areas over the surface of approximately several tens of unit cells, but significant long-range order was not observed (Baker et al., 1997, 1998).

MATERIALS AND METHODS

Sample preparation

Valonia ventricosa was harvested from a seabed in the Florida Keys. The microcrystals were prepared according to the method of Revol et al. (1982).

The cellulose fragments (initial concentration 1% w/w) were disintegrated in a Nissei AM3 homogenizer. Sulfuric acid was then added slowly to the suspension of the fragments to achieve a final acid concentration of 65% (w/w). The use of sulfuric acid improves the dispersion because of the slight surface charge given to the crystallites. The internal structure of the crystallites is known from electron diffraction experiments to be unaltered by this treatment (Sugiyama et al., 1992). The mixture was then heated to 70°C under strong stirring for 30 min. The resultant dispersion was washed with distilled water by successive centrifugation steps, until a cloudy supernatant was observed. A final ultrasonication step was used to complete the dispersion, and a drop of chloroform was added before the preparation was stored.

For atomic force microscopy, the dispersions were diluted again around 100-fold with ultrapure water, and a 5-μl drop of the suspension was deposited onto APTES-mica, which had been prepared by exposing the mica surface to an atmosphere of 3-aminopropyltriethoxysilane for several hours.

Received for publication 20 January 2000 and in final form 17 April 2000.

Address reprint requests to Dr. Andrew A. Baker, H. H. Wills Physics Laboratory, University of Bristol, Bristol BS8 1TL, UK. Tel.: 44-117-928-8743; Fax: 44-117-925-5624; E-mail: andy.baker@bristol.ac.uk.

© 2000 by the Biophysical Society

0006-3495/00/08/1139/07 $2.00

Atomic force microscopy

A Digital Instruments (Santa Barbara, CA) NanoScope III controller with a MultiMode AFM head was used to image the cellulose crystals, using the supplied liquid cell filled with water. Images were acquired in contact mode, using commercial, unmodified silicon nitride cantilevers with a nominal spring constant of 0.06 Nm^{-1}. Topographic and error-signal images were recorded simultaneously. Error-signal images enhance the high spatial frequency components in the image and can offer improved contrast for high-resolution imaging (Putman et al., 1992; Baker et al., 1997). Scan rates were typically 10–20 Hz, with the scan angle varied to obtain optimum contrast. The images are presented with the fast-scan direction of the cantilever oriented horizontally. The double-headed arrows shown in some images indicate the directions of the molecules along the crystal long axis. No filtering was used during scanning.

Image processing

The images presented are raw, unprocessed data, except for flattening and plane fitting to remove background slope (where appropriate). The only significantly processed image is the enlargement of part of Fig. 4 *A*, shown in Fig. 4 *C*, which has been rotated to align the cellulose chains vertically. Fourier filtering was also used to enhance the periodic features, which are clearly discernible in the original unprocessed image, to allow an easier comparison with the images derived from the computer modeling.

For comparison with the simulated image in Fig. 4 *D*, the AFM image shown in Fig. 4 *C* was calibrated using the known spacing along the chains between the covalently linked glucose units, such that the cellobiose repeat (1.04 nm) is identical in the two images. This calibration was performed isotropically, without attempting to correct for other scanner inaccuracies and distortions, which can be more prevalent in high-resolution imaging.

Computer modeling

The cellulose crystal models were built in Cerius^2 (Molecular Simulations Inc.) from the atomic coordinates of Sugiyama et al. (1991), which had been further characterized by molecular dynamics simulations (Heiner et al., 1995), with hydrogen atoms added at positions that maximize hydrogen bonding within the crystal (Baker, 1998). Crystal surfaces were then cleaved from these bulk structures, and the Connolly surface (Connolly, 1983) generation algorithm in the Cerius^2 program was used to produce a surface mimicking an AFM topographic image (Kuutti et al., 1994; Baker et al., 1998). This hard sphere analysis is not a dynamic simulation of the compliant surface under the influence of a real imaging tip, but it nevertheless allows the spatial positions of the groups on the surface to be compared easily with the real image, in both real and reciprocal space. The size of the probe rolling over the surface in the figures presented here was 0.2 nm, comparable to the size of a water molecule—larger probe sizes simply smoothed the surface and revealed less detail but did not obscure the key structural features of the surface. The size of the probe is considerably smaller than the 20–50-nm average radius of a typical AFM tip, but the high resolution of the images obtained is very likely due to the presence of much smaller microasperities at the end of the tip. The generated surfaces were exported to custom-written software to convert the surface coordinates into a simulated AFM topographic image with false-color height mapping.

RESULTS AND DISCUSSION

Fig. 1 shows simultaneously acquired topographic and error-signal (Putman et al., 1992) AFM images from the surface of a *Valonia* cellulose microcrystal. There are con-

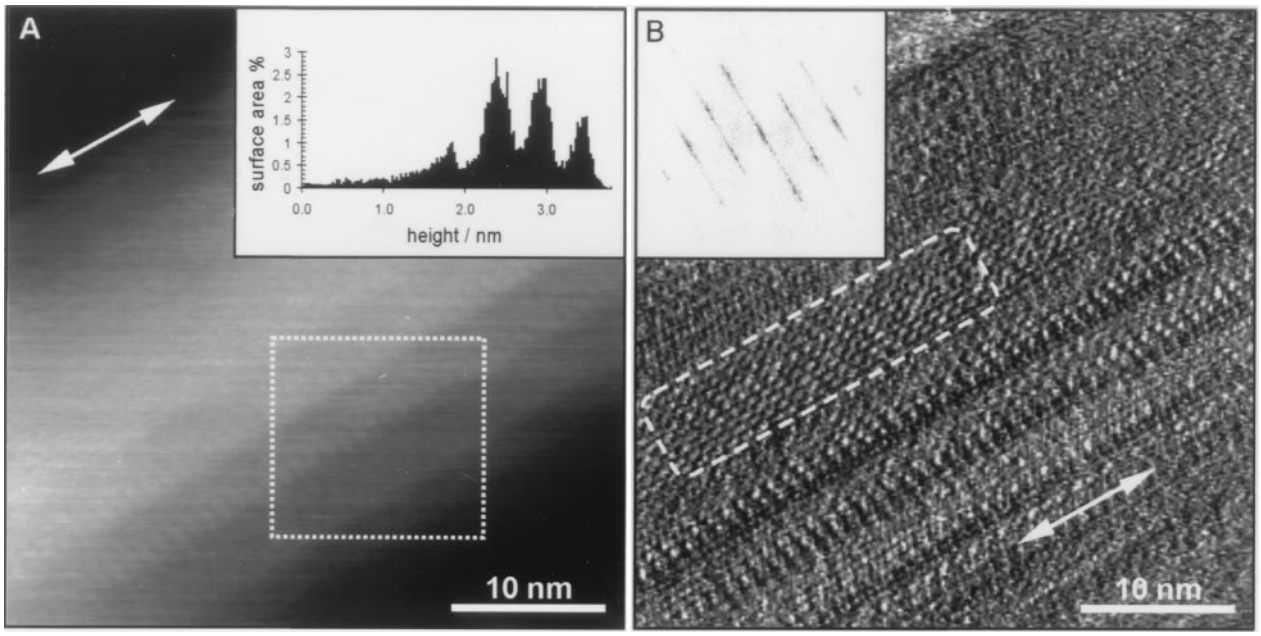

FIGURE 1 Simultaneous topographic (*A*) and error-signal (*B*) AFM images of a cellulose microcrystal from *Valonia*. In *A* there are steps at the edge of the crystal. The inset graph shows a histogram of the distribution of pixel heights over the area of the image marked by the dotted white box—four peaks spaced at 0.5–0.6 nm indicate that the steps are due to the removal of single layers of cellulose chains. In *B* the error-signal image emphasizes the high-resolution features on the surface, most notably within the white rectangular box. The pattern of spots within this box is characteristic of the I_α (triclinic) crystalline allomorph. The inset fast Fourier transform (FFT) shows the distinguishing triclinic signature seen in diffractograms. The slightly diffuse appearance of the high-intensity peaks of the FFT is due to alignment shifts in different parts of the image, as a consequence of both the crystal steps and the mechanical nature of the piezoelectric scanning system.

spicuous steps at the edge of the crystal, an observation made for many different crystals. These steps correspond to the spacing of the planes of cellulose molecules in the crystal; the *d*-spacing of the triclinic (100) and (010) planes is 0.62 and 0.53 nm, respectively. It is not clear whether these steps are present naturally or have been created by stripping away chains during the isolation and purification of the microcrystals. Cross sections through microcrystals imaged by transmission electron microscopy show a variety of shapes (Revol, 1982), and it is likely that the native fibrils do not always have perfectly sharp corners, contrary to the impression sometimes given by simple models.

The error-signal image in Fig. 1 *B* reveals even more detail at the surface, because the high spatial frequencies in the image are intensified along the horizontal fast-scan direction of the probe (Baker et al., 1997, 1998). The steps are still identifiable, although there is no indication that these are actually due to regular height changes. More importantly, the parallel molecular chains are now easily resolved, with detailed substructure visible along their length. The rectangular box indicates an area of particular clarity, removed from the steps at the edge, where a band over 10 molecules wide shows exceptional detail. The period of the features along the chains is 1.09 nm, closely matching the cellobiose interval. This interval is due to the twofold screw symmetry, where the alternate glucose subunits spaced at 0.52 nm are oriented to show either the C2-C3 or the O5-C5 face of the glucose ring. When the O5-C5 face is uppermost, the C6 hydroxyl group on the C5 carbon of the ring, which is oriented outward into the solvent, is a prominent topographic feature presented to the scanning tip of the microscope. This fact enables us in principle to distinguish between the monoclinic and triclinic motifs: the "bands" oriented diagonally at ~60° to the molecular axis are characteristic of the triclinic structure.

Fig. 2 *A* shows a stick representation of the molecular structure of cellulose I_α at the triclinic (100) surface, with the inset describing the glucose ring nomenclature. The small circle highlights the O6 oxygen atom that is part of the exocyclic hydroxymethyl group on the C5 carbon. The diagonal alignment is unmistakable, with the *c*/4 displacement of the chains bringing every fourth chain back into horizontal registry with the starting position. We have compared the AFM images with all four faces from the two proposed crystal models, using simulated AFM images constructed from the crystal-model surfaces. Fig. 2 *B* shows the same triclinic (100) crystal face as a topographic image. A qualitative comparison of the inset fast Fourier transform with the one shown with the image in Fig. 1 *B* immediately indicates the overall similarity with the real AFM images and confirms that the triclinic phase has been imaged.

Two error-signal images from different crystals are shown in Fig. 3. Fourier transforms of the data are shown to the right of each image—both of these show clearly defined peaks extending out for five diffraction orders to 0.17 nm. No filtering or other image processing has been used to enhance these images. This unprecedented resolution and the sharpness of the peaks are seen particularly in the real

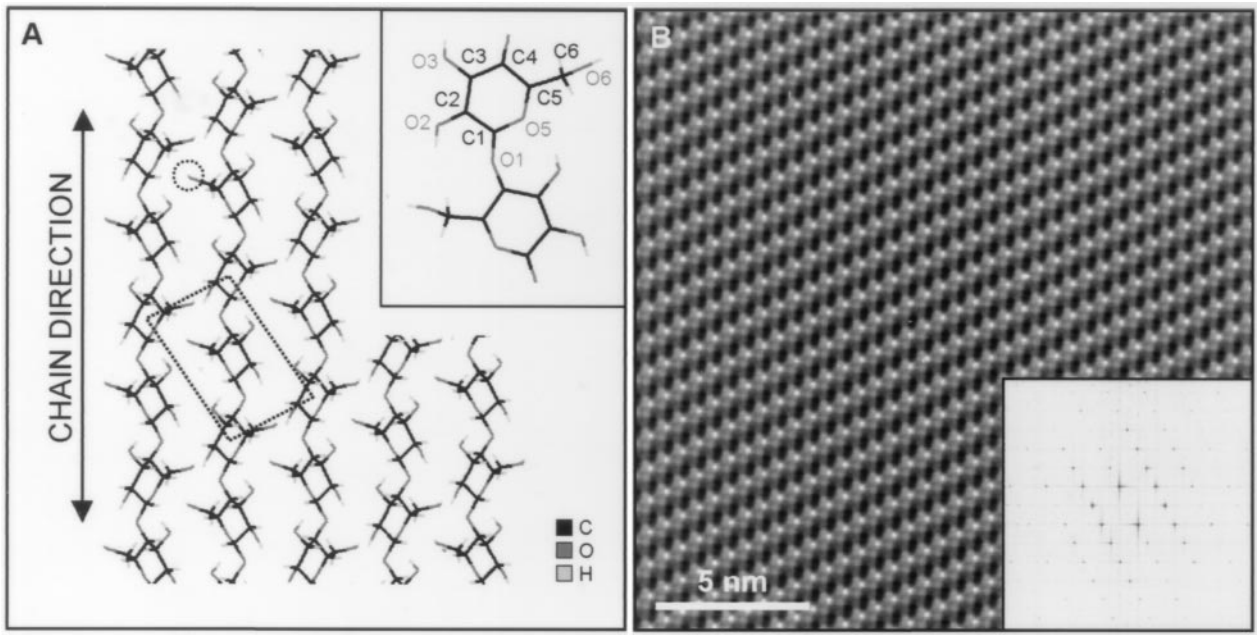

FIGURE 2 Model of the (100) face of the single-chain P1 triclinic structure. The dotted circle marks the O6 atom of the hydroxymethyl group. The parallelogram indicates the unit cell. The inset is a diagram of a single cellobiose unit, defining the ring nomenclature. (*B*) A simulated topographic AFM image of the (100) face from the crystal model in *A*. The inset shows the FFT of this crystal face. The triclinic (010) face (not shown) that may also be exposed to the imaging probe has a lower density of chain packing.

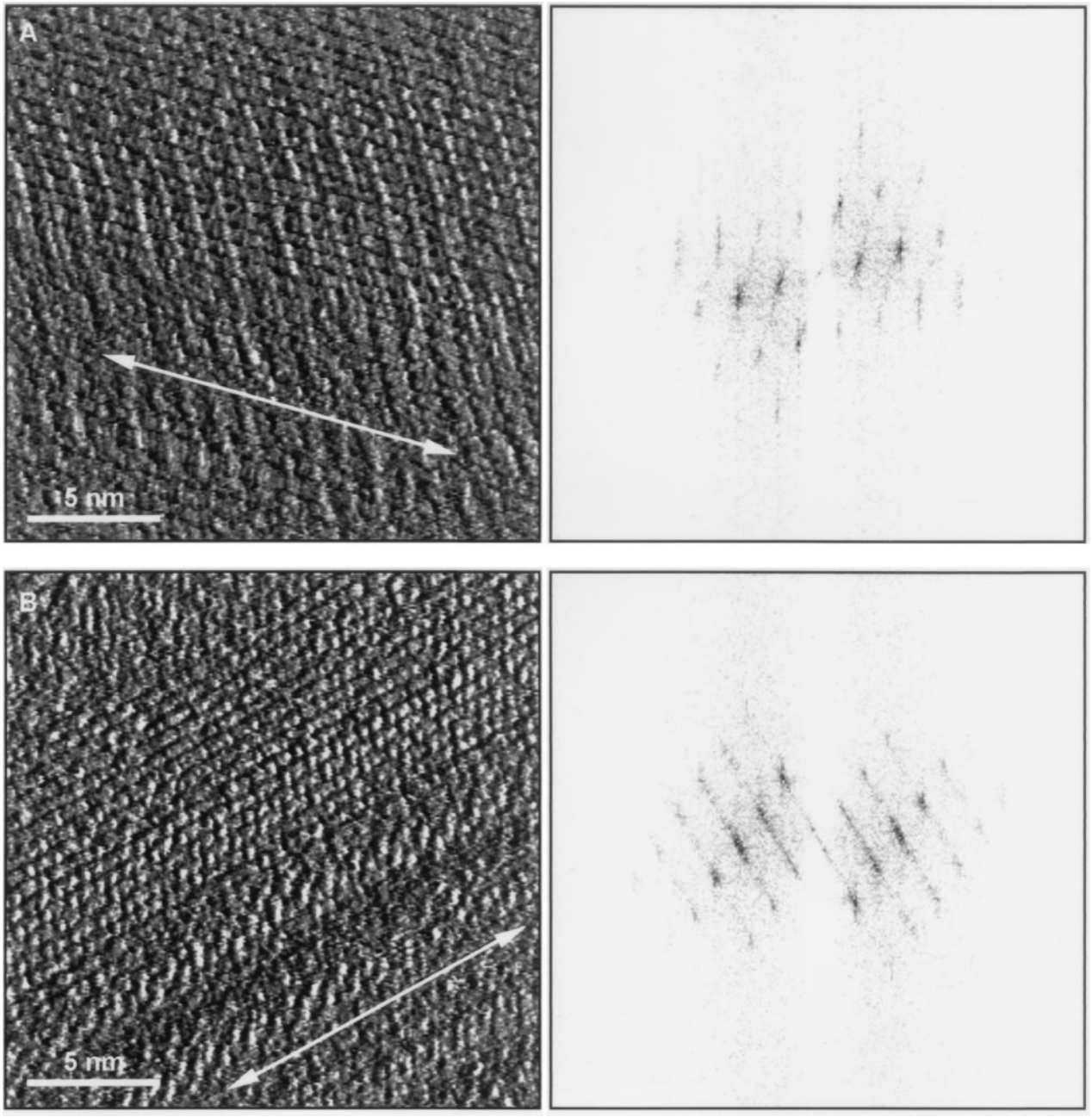

FIGURE 3 Error-signal images taken under water from two different microcrystals. *A* and *B* clearly show the triclinic structure seen in Fig. 2 *B* over large areas of the image. The fast-scan direction of the tip is horizontal, and the chain direction is indicated by the arrows. To the right of each image are FFTs of the data, similar to the many electron diffractograms published in the literature, showing the triclinic pattern. The peaks in the FFTs extend out for five orders to 0.17 nm.

space image in Fig 3 *A*, where there is excellent alignment of the chains over almost the entire 20 × 20 nm image, an area comparable with the width of the microcrystals. The triclinic order is evidently preserved over many hundreds of unit cells, a significant observation because diffraction techniques are unable to give such localized information about the size of I_α and I_β domains.

Fig. 4 highlights the compelling agreement between the real and model images. The bands indicating the triclinic phase and the twofold screw symmetry are easily seen in both the height image (Fig. 4 *A*) and error-signal image (Fig. 4 *B*). In Fig. 4 *C* the boxed area shown in Fig. 4 *A* has been enlarged and rotated to align the chains vertically. The image was Fourier filtered before enlargement, and only the clearly defined spectral peaks identified in the Fourier transform were preserved—high-frequency noise was therefore eliminated, and distracting, low-frequency topographic changes were removed to leave a planar surface. In Fig. 4 *D*,

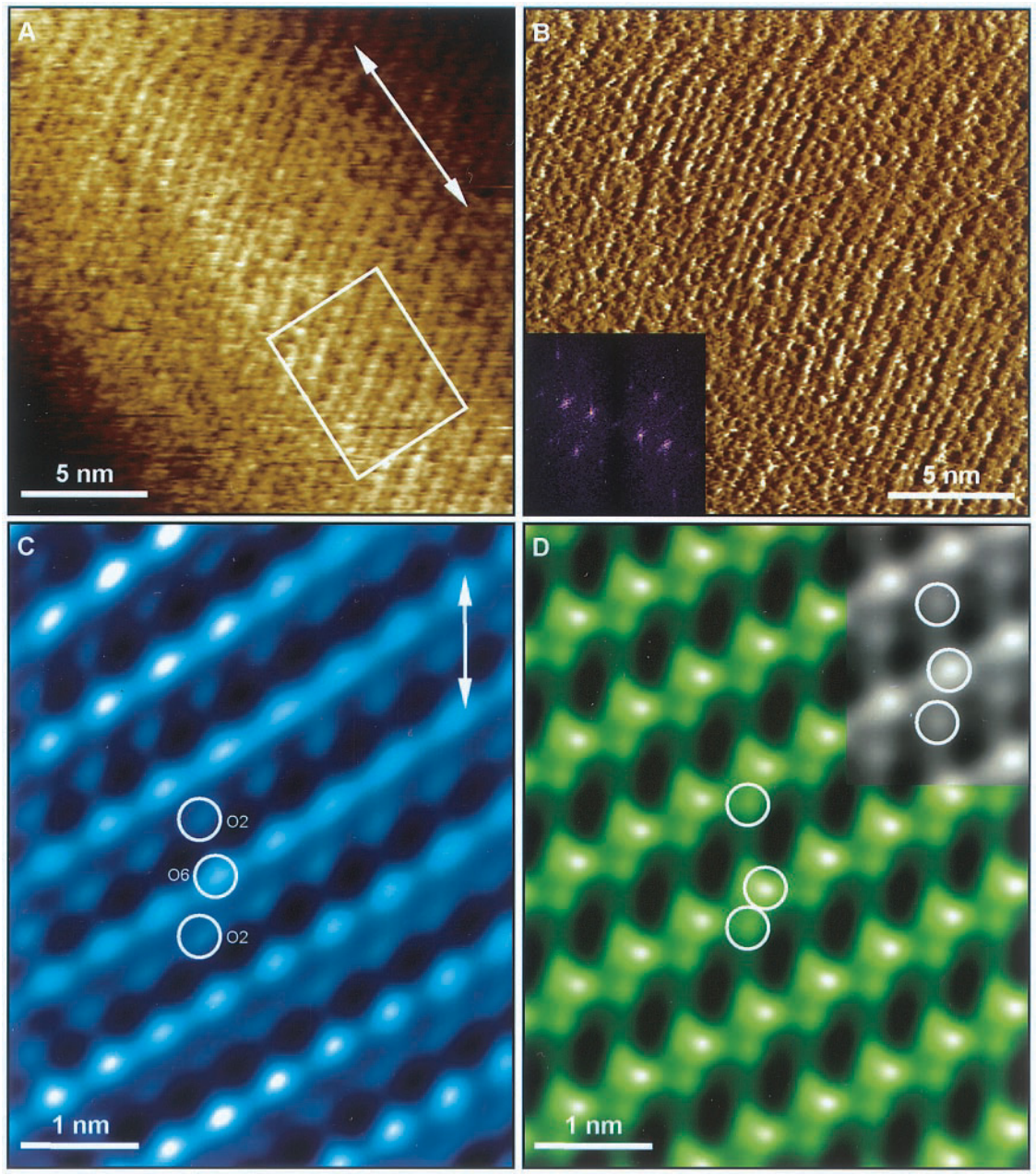

FIGURE 4 A comparison of real and simulated AFM images of the cellulose surface. The topographic image in *A* was acquired simultaneously with the error-signal image in *B*. (*C*) The boxed area in *A*, after filtering, enlargement, and rotation to align the chains vertically. The three circles indicate examples of peaks due to O2, O6, and O2. O6 is displaced slightly to the right of the two O2 peaks and is sited almost midway between them. The secondary O2 peak is lower in height than the O6 peak and is due to the C2 hydroxyl group or possibly to the combined effects of adjacent C2 and C3 hydroxyls. (*D*) The simulated AFM image shown in Fig. 2 *B* has been enlarged and low-pass filtered to allow comparison with *C*. In this model, with the C6-O6 group in a *tg* position expected in the crystal bulk, O6 is located very close to O2. The gray inset shows the effect of rotating O6 into a *gt* position, with the result that O6 is closer to being equidistant between the O2 groups. The model in gray clearly compares more favorably with the AFM image in *C*. The spacing between the chains on the two images is slightly different, as evidenced by the change in angle of the triclinic pattern by ~5°. Other images show similar deviations in the other direction due to scanning aberrations.

the simulated topographic image of the surface shown in Fig. 2 has been enlarged to the same magnification and low-pass filtered to restrict the spatial frequency range to be similar to the processing applied to the image in Fig. 4 *C*. The correspondence between these images is startling. The 1.04-nm cellobiose repeat is immediately obvious and is indicated in Fig. 4 *C* by the length of the arrowed line. A circle on the real image (*blue*) marks a high peak due to O6 of the hydroxymethyl group, with two O2 groups encircled above and below, displaced slightly to the left. The circles

drawn on the simulated image (*green*) show that O6 is positioned rather closer to O2 than it is in the real image. The exact position of these points depends on the torsional angles of the hydroxyl groups and the positions of the hydrogen atoms—the model in Fig. 4 *D* uses hydrogen atoms positioned to achieve maximum hydrogen bonding within the bulk crystal, where the hydroxymethyl is in the *tg* conformation. (The conformation of the O6 hydroxymethyl group is defined by two characters. The first refers to the O5-C5-C6-O6 torsion angle, and the second to the C4-C5-C6-O6 angle. Possible conformations are *gg*, *gt*, and *tg*, where *g* is *gauche* and *t* is *trans*.) Detailed molecular dynamics simulations elsewhere have studied the influence of water on the cellulose surface structure (Heiner et al., 1998; Kroon-Batenburg and Kroon, 1990; Heiner and Teleman, 1997). In water, the *tg* conformation favored in the bulk is less populated than the preferred *gauche* states. Solid-state ^{13}C NMR also suggests that the cellulose surface will be more mobile than in the crystal and that a *gt* conformation may be more predominant at the surface (Newman and Hemmingson, 1994). The gray inset in Fig. 4 *D* shows the effect of rotating the hydroxymethyl group around the C5-C6 bond into a *gt* position, and it is noticeable that the position of the surface groups more closely represents the organization in Fig. 4 *C*, which may be seen by comparing the positions of the circles drawn on the images. Similarly, the *gg* position (not shown) also makes a better comparison with the AFM data. Other modifications with the remaining hydroxyl groups and backbone torsions may also be considered, although the most significant effect is seen with O6, because of the additional distance from the ring afforded by the CH_2 linker. We suggest that, in the particular example shown here and under these imaging conditions, it is likely that the hydroxymethyl group is in a different position on the hydrated surface compared with the region inside the crystal. There are other possible effects that may contribute to our observation, but the data presented here are exciting, because for the first time they demonstrate visually these types of surface reconstruction for cellulose and that AFM is capable of resolving these intricacies.

The degree of topographic modulation between and along the chains also shows impressive agreement. The tight lateral packing of the chains is exemplified in Fig. 4, *C* and *D*, by the fact that the probe does not penetrate deeply between the chains. Along the chains, topographic variation is much greater. Careful analysis of the seven best images taken from two different crystals shows that the dimensions on all of the images correspond most closely with the triclinic (100) face (Baker, 1998). The interchain spacing is always closer to the d_{010} spacing of 0.53 nm, corresponding to an angle on the surface of 63° for the (100) face, compared to d_{100} on the (010) face where the chains spaced at 0.62 nm produce a larger angle of 67°. The (100) face is expected to be seen more frequently in AFM images due to the well-described "uniplanar orientation" phenomenon for these *Valonia* microcrystals, where the majority of the microcrystals have the (100) face oriented parallel to the mica support substrate (Sugiyama et al., 1984). Although the results reported here are encouraging in that respect, they are not statistically significant, and more crystals would need to be analyzed to confirm this result.

If native cellulose has two crystalline allomorphs, should we not also see the I_β (monoclinic) phase at the surface? Other authors have reported the monoclinic structure, although their images, obtained in air, are far less clear, and the expected real-space motif was not discerned (Kuutti et al., 1994). Acquiring high-quality images where structure can be clearly identified takes considerable time, and at present there are insufficient data to statistically apportion images of the crystals to the two phases. Interestingly, there is an increasing body of evidence from other techniques that the size and location of the triclinic and monoclinic nanodomains are species dependent. A recent electron microdiffraction study suggested that the monoclinic phase might exist at the interface between triclinic regions (Imai and Sugiyama, 1998). If this is the case, the surface may only be composed of the I_α phase, so that there is actually very little I_β present on the surface. Furthermore, after enzymic degradation or acetylation of *Valonia*, there is an increase in the proportion of the I_β phase (Hayashi et al., 1998a,b; Sassi, 1995), which may suggest that the I_α phase is more abundant at the surface. These questions certainly require further investigation.

In general, AFM images of the surface of the *Valonia* microcrystals that we have examined do not show such extreme order over the entire surface (Baker et al., 1997). Within single images taken at lower magnification, regions of the surface with greater disorder are often seen. Results from NMR also indicate that the surface may, in general, be less ordered than the interior and that there is greater mobility at the surface, although the assignment of spectral peaks to surface and interior configurations is a complicated issue, and new interpretations are still being put forward (Wickholm et al., 1998; Newman, 1998). It is clear from the images presented that on some areas of the surface, the molecular chains are highly organized, as also suggested by the low surface reactivity of *Valonia* and bacterial cellulose (Verlhac et al., 1990). Indeed, the overall level of order on the truly native surface may be even greater still, as the sample preparation procedures may have disrupted some parts of the surface.

CONCLUSIONS

The most striking result that we have presented here is that the triclinic structure has been revealed directly in real space over very large areas of the crystal surface, where the degree of order is very high. The close correspondence between topographic models and real data is impressive, and, more-

over, the structural comparison between the bulk crystal and its surface demonstrates remarkable changes in the position of the exocyclic hydroxyls, presumably due to changes in hydrogen bonding when the surface is solvated. The precise role of the tip and the imaging conditions on this observation requires further investigation, but nevertheless we have clearly demonstrated near-atomic resolution on this important biological specimen. Understanding the relationship between biosynthesis and structure remains one of the most important goals in cellulose research, where scanned probe techniques will surely continue to play an exciting role.

We thank Dr. H. Chanzy and Dr. T. J. McMaster for their critical appraisals of the manuscript and for helpful discussions.

REFERENCES

Atalla, R. H., and D. L. VanderHart. 1984. Native cellulose: a composite of two distinct crystalline forms. *Science.* 223:283–285.

Baker, A. A. 1998. High resolution atomic force microscopy of polysaccharides. Ph.D. thesis. University of Bristol.

Baker, A. A., W. Helbert, J. Sugiyama, and M. J. Miles. 1997. High resolution AFM of native cellulose. I. *Valonia* microcrystals. *J. Struct. Biol.* 119:129–138.

Baker, A. A., W. Helbert, J. Sugiyama, and M. J. Miles. 1998. Surface structure of native cellulose microcrystals by AFM. *Appl. Phys. A.* 66:S559–S563.

Connolly, M. L. 1983. Solvent-accessible surfaces of proteins and nucleic acids. *Science.* 221:709–713.

Hayashi, N., J. Sugiyama, T. Okano, and M. Ishihara. 1998a. Selective degradation of the cellulose I_α component in *Cladophora* cellulose with *Trichoderma viride* cellulase. *Carbohydr. Res.* 305:109–116.

Hayashi, N., J. Sugiyama, T. Okano, and M. Ishihara. 1998b. The enzymatic susceptibility of cellulose microfibrils of the algal-bacterial type and the cotton-ramie type. *Carbohydr. Res.* 305:261–269.

Heiner, A. P., L. Kuutti, and O. Teleman. 1998. Comparison of the interface between water and four surfaces of native crystalline cellulose by molecular dynamics simulations. *Carbohydr. Res.* 306:205–220.

Heiner, A. P., J. Sugiyama, and O. Teleman. 1995. Crystalline cellulose I_α and I_β studied by molecular dynamics simulation. *Carbohydr. Res.* 273:207–223.

Heiner, A. P., and O. Teleman. 1997. Interface between monoclinic crystalline cellulose and water: breakdown of the odd/even duplicity. *Langmuir.* 13:511–518.

Horii, F., H. Yamamoto, and A. Hirai. 1997. Microstructural analysis of microfibrils of bacterial cellulose. *Macromol. Symp.* 120:197–205.

Imai, T., and J. Sugiyama. 1998. Nanodomains of I_α and I_β in algal microfibrils. *Macromolecules.* 31:6275–6279.

Kroon-Batenburg, L. M. J., and J. Kroon. 1990. Solvent effect on the conformation of the hydroxymethyl group established by molecular dynamics simulations of methyl-D-glucoside in water. *Biopolymers.* 29:1243–1248.

Kuutti, L., J. Peltonen, J. Pere, and O. Teleman. 1994. Identification and surface structure of crystalline cellulose studied by atomic force microscopy. *J. Microsc.* 178:1–6.

Newman, R. H. 1998. Evidence for assignment of ^{13}C NMR signals to cellulose crystallite surfaces in wood, pulp and isolated celluloses. *Holzforschung.* 52:157–159.

Newman, R. H., and J. A. Hemmingson. 1994. Carbon-13 NMR distinction between categories of molecular order and disorder in cellulose. *Cellulose.* 2:95–110.

Putman, C. A. J., K. van der Werf, B. G. de Grooth, N. F. van Hulst, J. Greve, and P. K. Hansma. 1992. A new imaging mode in AFM based on the error signal. *Proc. SPIE.* 1639:198–204.

Revol, J.-F. 1982. On the cross-sectional shape of cellulose crystallites in *Valonia ventricosa. Carbohydr. Polym.* 2:123–134.

Sarko, A., and R. Muggli. 1974. Packing analysis of carbohydrates and polysaccharides. III. *Valonia* cellulose and cellulose II. *Macromolecules.* 7:486–494.

Sassi, J.-F. 1995. Etude ultrastructurale de l'acétylation de la cellulose application à la préparation de nanocomposites. Ph.D. thesis. Université Joseph Fourier, Grenoble, France. 57–73.

Sugiyama, J., H. Chanzy, and G. Maret. 1992. Orientation of cellulose microcrystals by strong magnetic fields. *Macromolecules*. 25: 4232–4234.

Sugiyama, J., H. Harada, Y. Fujiyoshi, and N. Uyeda. 1984. High resolution observations of cellulose microfibrils. *Mokuzai Gakkaishi.* 30: 98–99.

Sugiyama, J., T. Okano, H. Yamamoto, and F. Horii. 1990. Transformation of *Valonia* cellulose crystals by an alkaline hydrothermal treatment. *Macromolecules.* 23:3196–3198.

Sugiyama, J., R. Vuong, and H. Chanzy. 1991. Electron diffraction study on the two crystalline phases occurring in native cellulose from an algal cell wall. *Macromolecules.* 24:4168–4175.

VanderHart, D. L., and R. H. Atalla. 1984. Studies of microstructure in native celluloses using solid-state ^{13}C NMR. *Macromolecules.* 17: 1465–1472.

Verlhac, C., J. Dedier, and H. Chanzy. 1990. Availability of surface hydroxyl groups in *Valonia* and bacterial cellulose. *J. Polym. Sci. A.* 28:1171–1177.

Wickholm, K., P. T. Larsson, and T. Iverson. 1998. Assignment of non-crystalline forms in cellulose I by CP/MAS ^{13}C NMR spectroscopy. *Carbohydr. Res.* 312:123–129.

Yamamoto, H., F. Horii, and H. Odani. 1989. Structural changes of native cellulose crystals induced by annealing in aqueous alkaline and acidic solutions at high temperatures. *Macromolecules.* 22:4130–4132.